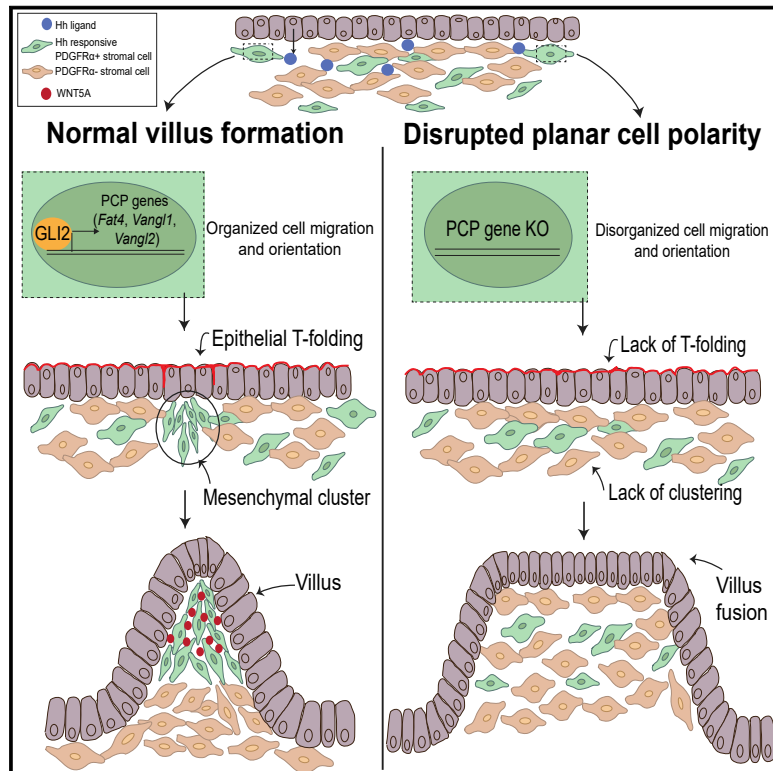


Developmental Cell

Hedgehog-Activated Fat4 and PCP Pathways Mediate Mesenchymal Cell Clustering and Villus Formation in Gut Development

Graphical Abstract



Authors

Abilasha Rao-Bhatia, Min Zhu, Wen-Chi Yin, ..., Helen McNeill, Sevan Hopyan, Tae-Hee Kim

Correspondence

tae-hee.kim@sickkids.ca

In Brief

Rao-Bhatia et al. investigate the signaling mechanisms of cell behavior during mammalian villus morphogenesis. They demonstrate that Hh signaling in the intestinal mesenchyme directly activates planar cell polarity genes, thereby regulating the stromal cell clustering behavior required for epithelial remodeling in villus formation.

Highlights

- Hh activates planar cell polarity genes in the developing intestinal mesenchyme
- *Fat4* pathway is required for proper mesenchymal clustering in villus formation
- Planar cell polarity mechanisms ensure organized stromal cell behavior
- Stromal clustering through planar polarity is required for villus demarcation



Hedgehog-Activated Fat4 and PCP Pathways Mediate Mesenchymal Cell Clustering and Villus Formation in Gut Development

Abilasha Rao-Bhatia,^{1,2} Min Zhu,^{1,3} Wen-Chi Yin,^{1,2} Sabrina Coquenlorge,^{1,2} Xiaoyun Zhang,^{1,2} Janghee Woo,^{4,5} Yu Sun,³ Charlotte H. Dean,⁶ Aimin Liu,⁷ Chi-chung Hui,^{1,2} Ramesh A. Shivdasani,^{4,5} Helen McNeill,^{2,8} Sevan Hopyan,^{1,2} and Tae-Hee Kim^{1,2,9,*}

¹Program in Developmental & Stem Cell Biology, the Hospital for Sick Children, Toronto, ON M5G 0A4, Canada

²Department of Molecular Genetics, University of Toronto, Toronto, ON M5S 1A8, Canada

³Department of Mechanical and Industrial Engineering, University of Toronto, Toronto, ON M5S 3G8, Canada

⁴Department of Medical Oncology and Center for Functional Cancer Epigenetics, Dana-Farber Cancer Institute, Boston, MA 02215, USA

⁵Department of Medicine, Harvard Medical School, Boston, MA 02215, USA

⁶Inflammation, Repair and Development Section, National Heart and Lung Institute, Imperial College London, London, UK

⁷Department of Biology, Eberly College of Science, Centers for Cellular Dynamics and Molecular Investigation of Neurological Disorders, Huck Institute of Life Sciences, The Pennsylvania State University, University Park, PA 16802, USA

⁸Department of Developmental Biology, Washington University School of Medicine, St. Louis, MO 63110, USA

⁹Lead Contact

*Correspondence: tae-hee.kim@sickkids.ca

<https://doi.org/10.1016/j.devcel.2020.02.003>

SUMMARY

During development, intestinal epithelia undergo dramatic morphogenesis mediated by mesenchymal signaling to form villi, which are required for efficient nutrient absorption and host defense. Although both smooth-muscle-induced physical forces and mesenchymal cell clustering beneath emerging villi are implicated in epithelial folding, the underlying cellular mechanisms are unclear. Hedgehog (Hh) signaling can mediate both processes. We therefore analyzed its direct targetome and revealed *GLI2* transcriptional activation of atypical cadherin and planar cell polarity (PCP) genes. By examining *Fat4* and *Dchs1* knockout mice, we demonstrate their critical roles in villus formation. Analyses of PCP-mutant mice and genetic interaction studies show that the *Fat4-Dchs1* axis acts in parallel to the core-*Vangl2* PCP axis to control mesenchymal cell clustering. Moreover, live light-sheet fluorescence microscopy and cultured PDGFR α + cells reveal a requirement for PCP in their oriented cell migration guided by WNT5A. Therefore, mesenchymal PCP induced by Hh signaling drives cell clustering and subsequent epithelial remodeling.

INTRODUCTION

The intestine is a remarkable organ, comprising millions of finger-like projections termed villi. These structures are critical for maximizing nutrient absorption and serve as a protective barrier to harmful pathogens. Compromised villi have been associated with serious diseases including malabsorption, short bowel syndrome, and intestinal failure (Walton et al., 2016a). These condi-

tions are treated with intravenous nutritional supplements or, in severe cases, intestinal transplants. A better understanding of the mechanisms underlying villus morphogenesis would provide possible treatment options aimed instead at villus regeneration.

During mid-embryogenesis, the primitive gut tube consists of a layer of pseudostratified epithelium with an underlying mesenchymal compartment. The cross-talk of these apposed tissues is crucial for proper gastrointestinal development (Le Guen et al., 2015). In a dramatic transformation known as villification, the smooth pseudostratified epithelium is extensively remodeled, resulting in protrusions of prospective villi lined by a columnar epithelium. Two distinct models have been proposed to explain this complex morphogenesis. The first model, supported by chick explant studies, demonstrated that physical forces generated by smooth muscle are essential and even sufficient to trigger epithelial folding; mouse intestinal explants treated with muscle inhibitors also failed to undergo villification (Shyer et al., 2013). The second model, supported by mouse genetic studies, involves highly regulated patterning events (Karlsson et al., 2000; Walton et al., 2012, 2016b). Not only does the epithelium experience reorganization, the underlying stroma undergoes substantial cell rearrangements in the form of organized cell clustering. Notably, these stromal cells begin to cluster in response to epithelial signals, correlated with the onset of villification, and appear patterned at the base of each emerging villus (Walton et al., 2016a). In this model, key developmental signaling pathways such as Bone Morphogenetic Protein (BMP), Platelet-derived growth factor (Pdgf), and Hedgehog (Hh) precisely pattern the mesenchymal clusters, forming a classic self-organizing Turing field (Karlsson et al., 2000; Walton et al., 2012, 2016b). Indeed, alterations in these pathways led to clustering defects and subsequent failure of villus formation (Karlsson et al., 2000; Walton et al., 2012, 2016b), but how these villus clusters are formed remains unclear.

Hh signaling is critical for both smooth muscle differentiation and mesenchymal cell clustering during gut development (Huang



et al., 2013; Mao et al., 2010; Ramalho-Santos et al., 2000; Walton et al., 2012). To stimulate the latter effect, Hh signaling would likely activate and/or coordinate with cell polarity and adhesion pathways. During development, a pair of very large cell adhesion molecules, Fat and Dachsous, mediate diverse morphogenetic processes through the regulation of planar cell polarity (PCP) and Hippo signaling (Blair and McNeill, 2018). For example, *Dchs1* and *Fat4* orchestrate kidney tubule formation and skeletal morphogenesis (Mao et al., 2011, 2016; Saburi et al., 2008) but their roles in intestinal villification are unexplored.

Owing to the instability of Hh downstream Glioma-associated oncogene (GLI) transcription factors, which are tightly controlled by negative regulators, Suppressor of fused (SUFU) and Speckle-type POZ protein (SPOP) (Briscoe and Therond, 2013; Wang et al., 2010), uncovering Hh downstream mechanisms has proven extremely difficult. To overcome this limitation, we conditionally deleted these Hh negative regulators and mapped GLI2 genomic binding regions, having successfully defined a Hh direct targetome in the intestinal mesenchyme (Coquenlorge et al., 2019). To define the cellular and transcriptional mechanisms of villification, we first analyzed our gut mesenchymal Hh targetome. Surprisingly, we identified *Fat4*, *Dchs1*, and other PCP genes as direct GLI2 targets. By analyzing mouse mutants for *Fat4*, *Dchs1*, and core PCP genes such as *Vangl2* and *Wnt5a* and performing complementary live-imaging and cell culture studies, we demonstrate that the *Fat4-Dchs1* signaling axis acts in parallel to the *Vangl2*-core PCP axis to induce PCP, which is essential for mesenchymal clustering behavior and villification.

RESULTS

PCP Pathway Genes Are Direct Targets of Hh Transcriptional Activator GLI2

Hh signaling is required for mesenchymal cell clustering, which allows epithelial remodeling during villus emergence, but it is unclear how the signal promotes organized stromal cell movement for clustering behavior. To address this question, we performed RNA sequencing (RNA-seq) of *Bapx1^{Crel/+};Sufu^{fl/fl};Spop^{fl/fl}* embryonic intestinal mesenchyme, where conditional deletion of Hh negative regulators *Sufu* and *Spop* in the gut stroma stabilizes GLI2-mediated gene activation (Wang et al., 2010) (Figure S1). Gene Ontology analysis of the significantly upregulated genes revealed an enrichment of “planar polarity”-related terms (Figure 1A; Table S1). Moreover, these terms appeared in a large cluster of neighboring terms, arranged based on similarity of biological function (Supek et al., 2011). Unsupervised hierarchical clustering of PCP genes identified many components enriched upon Hh activation (Figure 1B). These included genes such as *Vangl1*, *Vangl2*, and *Wnt5a*, from the core PCP pathway, as well as *Dchs1* and *Fat4*, from the atypical cadherin PCP pathway, which were validated by qPCR analysis (Figures 1B and 1C). To determine whether these genes are direct transcriptional targets of GLI2, we performed chromatin immunoprecipitation sequencing (ChIP-seq) (Coquenlorge et al., 2019) and demonstrated that GLI2 binds promoter and enhancer elements of a number of these genes (Figure 1D). Furthermore, these GLI2 binding sites were validated in an *in vitro* luciferase reporter assay, in which GLI2 binding regions of *Fat4*, *Vangl1*, and *Vangl2* were cloned upstream of the luciferase gene and co-transfected

with *Gli2* expression vectors into C3H10T1/2 cells (a mouse embryo fibroblast cell line). Reporter activity was indeed upregulated upon GLI2 expression compared to controls, demonstrating functional GLI2 responsiveness (Figure 1E). Together, these results demonstrate the GLI2-mediated direct transcriptional activation of PCP genes in response to Hh signaling in the developing intestinal mesenchyme.

Fat4-Dchs1 Signaling Axis Is Required for Proper Villification and Mesenchymal Clustering

Fat4 is involved in various types of mammalian morphogenesis (Cappello et al., 2013; Mao et al., 2011, 2016; Ragni et al., 2017; Saburi et al., 2008) but its role in villification is currently unknown. To determine whether *Fat4* is required for intestinal morphogenesis, we examined *Fat4* knockout (KO) intestines at embryonic day (E) 15.5, the stage at which villi begin to emerge. Notably, these *Fat4* KO intestines exhibited a striking morphological phenotype: scanning electron microscopy identified regions of the proximal intestine with distinct structural abnormalities and improperly patterned villi (Figure 2A). Histology revealed extensive fused villus regions (Figure 2B). To determine the status of mesenchymal clustering, we performed immunofluorescence staining for PDGFR α , a marker for mesenchymal clusters (Karlsson et al., 2000), and found a failure of stromal clustering beneath the fused villi, as shown by the disorganized and diffuse distribution of PDGFR α + cells (Figure 2C). Since previous reports have suggested that the muscle layer is critical for villification (Shyer et al., 2013), we also analyzed the formation of both circular and longitudinal muscle in our mutants and found no significant difference in their distribution and thickness (Figures S2A and S2B). To assess other mesenchymal cell types, we also quantified the percentage of α SMA+ cells in the lamina propria and observed no significant differences in *Fat4* KO compared to controls (Figures S2C and S2D), suggesting that the fusion phenotype is specific to the distribution of PDGFR α + cells in the mesenchyme. Furthermore, intestines deleted for *Dchs1*, another atypical cadherin known to interact with *Fat4* as a ligand to regulate signaling (Blair and McNeill, 2018; Mao et al., 2011), also exhibited extensive villus fusion and disrupted mesenchymal clustering (Figure 2D). Therefore, the entire *Dchs1-Fat4* signaling axis is required for villification and mesenchymal cluster formation.

Fat4 Acts Autonomously in the Villus Core for Mesenchymal Clustering and Villification

To understand the mechanisms by which *Fat4* mediates villification, we delineated *Fat4* expression patterns during intestinal villus emergence. Our qPCR analysis revealed an enrichment of some PCP genes, *Fat4*, *Dchs1*, and *Wnt5a*, in the mesenchyme (Figure 2E). Single-molecule fluorescent *in situ* hybridization (smFISH) revealed high *Fat4* mRNA levels in the mesenchymal villus core, which houses the clustering cells (Figures 2F and S3A). These cells were previously shown to be *Ptch1*+ and Hh responsive, further supporting *Fat4* as a Hh target gene (Walton et al., 2012). SmFISH confirmed that the expression of both *Fat4* and *Dchs1* was largely confined to the mesenchyme, whereas *Vangl1* and *Vangl2* were expressed in both epithelial and mesenchymal compartments (Figures 2F, 2G, and S3A). Moreover, VANGL2 immunofluorescence staining showed that a subset of PDGFR α + cells are positive for VANGL2 (Figure S3B). To

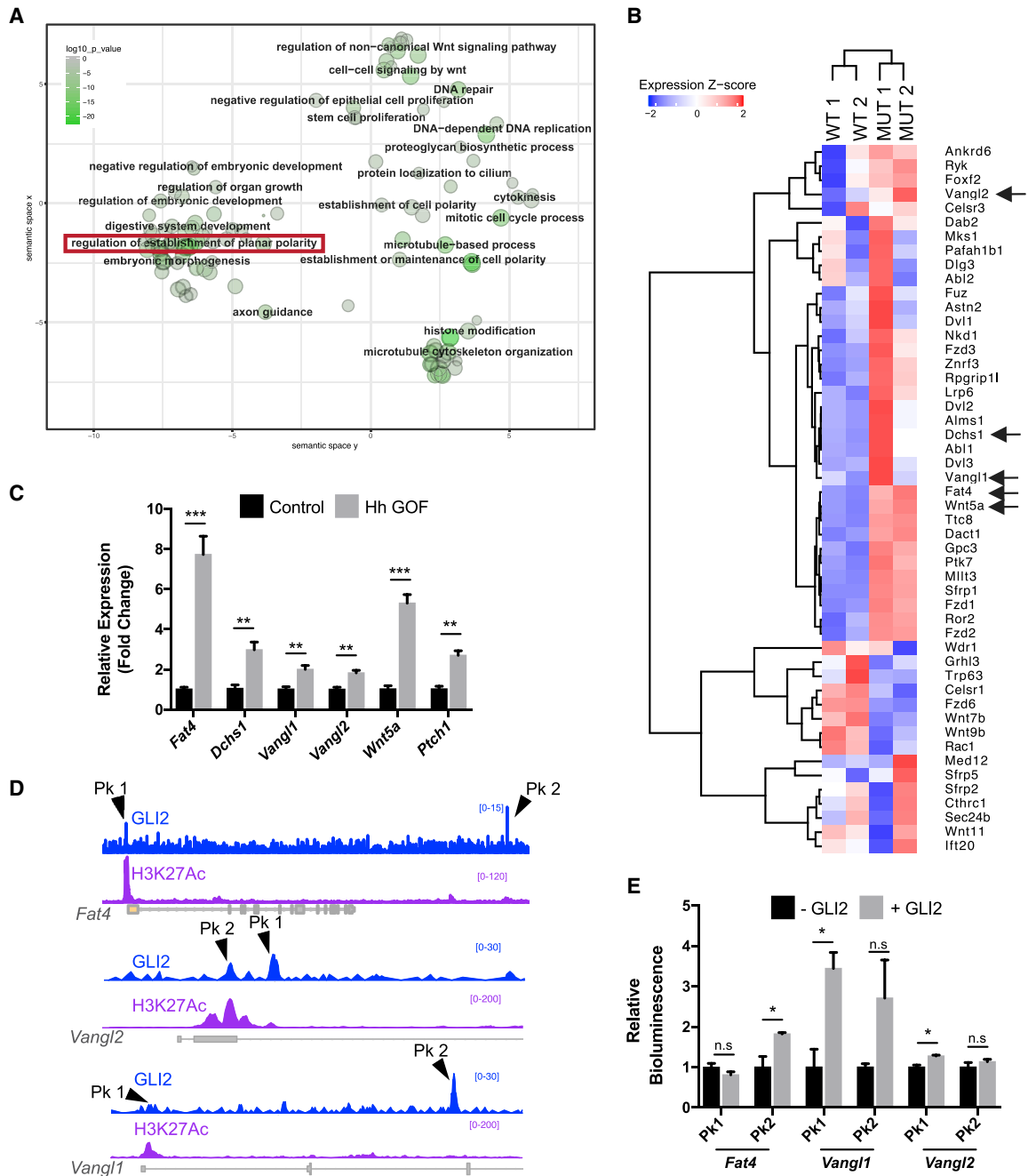


Figure 1. PCP Genes Are Direct Targets of the Hh Signaling Pathway in the Intestine during Villification

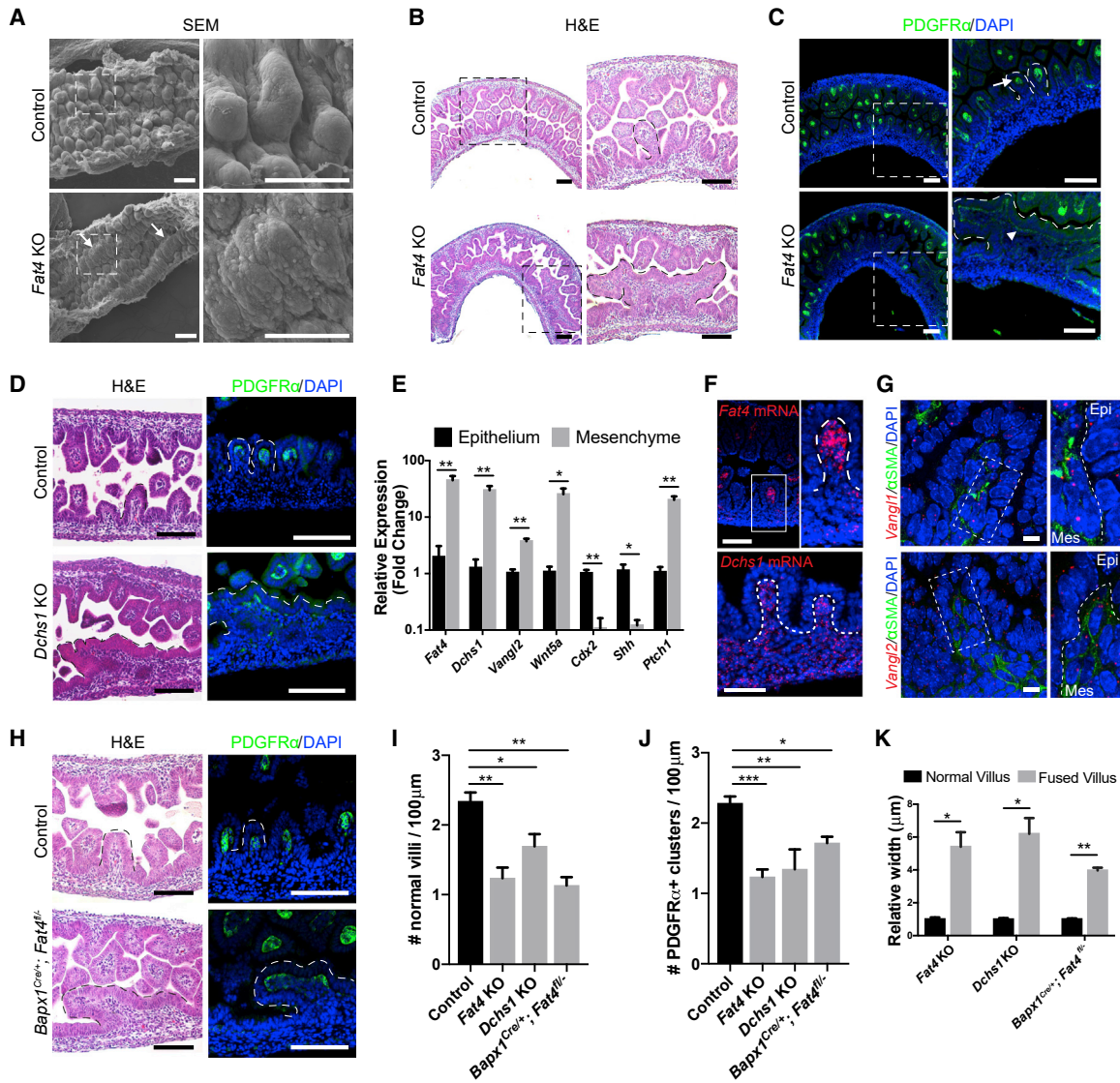
(A) Reduce and Visualize Gene Ontology (REVIGO) analysis scatterplot to visualize the top 300 upregulated Gene Ontology (GO) biological processes from RNA-seq of isolated mesenchymal cells from E17.5 *Bapx1^{Cre/+};Sufu^{fl/fl};Spop^{fl/fl}* embryos (Hh gain of function, see Figure S1) compared to controls. Each sphere represents a GO term and is plotted based on the similarity of biological function. Sphere size represents the proportion of genes that encompass the GO term. Red box indicates the “regulation and establishment of planar polarity” term. See Table S1 for all listed GO terms.

(B) Unsupervised hierarchical clustering of PCP genes from RNA-seq analysis of mesenchymal cells from E17.5 *Bapx1^{Cre/+};Sufu^{fl/fl};Spop^{fl/fl}* embryos (Hh gain of function) compared to controls. Arrows indicate examples from the core PCP pathway (*Vangl2*, *Vangl1*, and *Wnt5a*) and atypical cadherin-PCP pathway (*Fat4* and *Dchs1*) genes.

(C) Quantitative PCR of E15.5 *Bapx1^{Cre/+};Sufu^{fl/fl};Spop^{fl/fl}* mutants (Hh gain of function) for validation of upregulated PCP gene expression compared to controls (reported as \pm SEM, ** $p < 0.005$, *** $p < 0.0005$, $n = 4$).

(D) Visualization of GLI2 and H3K27Ac binding signals at *Fat4*, *Vangl2*, and *Vangl1* loci identified by ChIP-seq analysis of E17.5 *Bapx1^{Cre/+};Sufu^{fl/fl};Spop^{fl/fl}* (Hh gain of function) mutants. Arrows denote the peaks that were chosen to test functional GLI2 responsiveness and are labeled as “Pk1” and “Pk2.”

(E) Validation of GLI2 binding peaks for *Fat4*, *Vangl1*, and *Vangl2* regions measured as relative bioluminescence through firefly luciferase reporter activation in response to GLI2 overexpression and control Renilla luciferase activation (reported as mean \pm SEM; * $p < 0.05$; n.s., not significant; $n = 3$).



(legend continued on next page)

determine a tissue-specific role for *Fat4*, we deleted it in the intestinal mesenchyme using a *Bapx1^{Cre/+}* allele that specifically targets this tissue (Verzi et al., 2009). *Fat4* was effectively deleted in the mesenchyme of *Bapx1^{Cre/+};Fat4^{fl/-}* mice and showed similar villus fusions and disrupted mesenchymal clustering (Figures 2H and S3C). We found a significant decrease in the numbers of normal villi and PDGFR α + clusters per 100 μ m as well as a significant increase in the width of fused villi relative to normal villi (Figures 2I–2K), demonstrating that *Fat4* acts in mesenchymal cells to mediate clustering behavior and subsequent villus formation. To test if defects in proliferation impair mesenchymal clustering, we performed immunofluorescence staining for Proliferating Cell Nuclear Antigen (PCNA) but found no significant differences in the proportion of PCNA+ cells in the mesenchyme of the fusions compared to controls (Figures S3D and S3E). These results indicate that disrupted clustering and villus fusions are not due to proliferation defects.

Fat4 Signaling Mediates PCP and Acts in Parallel to the Core-PCP Axis to Induce Mesenchymal Clustering and Subsequent Epithelial Remodeling

Since *Fat4* signaling has been shown to regulate PCP and/or Hippo signaling (Blair and McNeill, 2018; Cappello et al., 2013; Ragni et al., 2017; Saburi et al., 2008), we sought to identify which of these downstream pathways mediates mesenchymal clustering. To determine whether villus fusion results from disruption of PCP, we analyzed mouse mutants defective in this pathway. *Wnt5a* is a known PCP ligand and mutants exhibit severe gut shortening (Cervantes et al., 2009) but its role in villification is unclear. Histologic analysis of *Wnt5a* KO mice revealed severe villus fusions in restricted areas, similar to the *Fat4* KO phenotype (Figure 3A). *Looptail* (*Vangl2^{Lp/Lp}*) (Montcouquiol et al., 2003) mutants also exhibited villus fusions in some areas (Figure 3A), revealing a requirement for the core PCP pathway in complete and proper villification. To examine the status of Hippo signaling in *Fat4* KO mice, we quantified the amounts of Yes-associated Protein (YAP) and phosphorylated YAP by western blot (Figures 3B, 3C, and S4). We also performed smFISH to quantify transcript abundance of the YAP target gene, *Ctgf* (Zhao et al., 2008) (Figures 3D and 3E). There were no significant differences in the relative levels of phosphorylated YAP nor were differences observed in *Ctgf* transcript levels between *Fat4* mutants and controls, indicating that Hippo signaling is intact in the absence of intestinal *Fat4*. Thus, villus fusion in *Fat4* KO mice likely reflects the loss of PCP rather than altered Hippo signaling.

To decipher the relationship between core-PCP and *Fat4*-PCP axes, we sought to determine whether these pathways act in parallel to maintain PCP or in a hierarchical manner. Indeed, when one copy of *Vangl2* was mutated in a *Fat4* KO background, the villus fusion defects were dramatically exacerbated, demonstrating their genetic interactions (Figures 3F and 3G). These results are also consistent with the report that the core-PCP and

Fat4-PCP axes act in parallel to maintain PCP during kidney morphogenesis (Saburi et al., 2008).

Having demonstrated the necessity of PCP in villification, we asked how defects in stromal clustering influence epithelial remodeling. Intestinal epithelial cells between mesenchymal clusters experience a circumferential force that causes mitotic rounding and eventual folding of the apical membrane into characteristic invaginations (T-folds) that demarcate villus boundaries (Freddo et al., 2016). Based on the villus fusion defects that follow when PCP is disrupted, we hypothesized that properly oriented mesenchymal clustering is required for epithelial remodeling into T-folds, thereby establishing villus boundaries. To examine this process, we performed immunostaining to visualize the protein EZRIN as a marker for the apical membrane, and found significantly fewer epithelial T-folds in *Fat4* KO mutants compared to littermate controls (Figures 4A–4C). Thus, villus demarcation requires properly oriented mesenchymal clustering, highlighting the role of stromal PCP in epithelial tissue remodeling.

Stromal PCP Regulates Organized Cell Clustering Behavior during Villification

Given the requirement of stromal PCP for clustering and subsequent epithelial remodeling for villification, we further investigated how PCP mediates this type of stromal cell behavior. To address this question, we used *Pdgfra^{H2B-eGFP}* mice, in which PDGFR α + clustering mesenchymal cells express a nuclear GFP reporter (Hamilton et al., 2003) and performed live imaging with light-sheet fluorescence microscopy to visualize clustering cell behavior *ex vivo* (Figure 5A). Through live cell tracking and analysis of GFP+ cell displacement over time, we observed organized migration of control PDGFR α + cells along the proximal-distal (P-D) axis, culminating in oriented clusters (Figures 5B–5D; Video S1). In *Fat4* mutants, by contrast, PDGFR α + cell migration was disorganized, lacking specific orientation (Figures 5B–5D; Video S2). Moreover, we could readily capture clustering behavior over 3 h of imaging time in the controls, while cluster formation was significantly impaired in *Fat4* mutants (Figures 5B and 5C). We also visualized dysregulated stromal cell behavior *in vivo* by staining F-actin networks. In the villus core of control intestines, stromal cells were oriented toward the dorsal-ventral (D-V) axis, while they were oriented along the P-D axis near the muscle layer (Figure 5E). However, cell orientation in *Fat4* mutants was disorganized, showing no axis preference at the core (Figure 5E). Together, these findings reveal *Fat4* as a critical regulator of cell migration and orientation.

PDGFR α + Cells Respond to WNT5A as a Chemoattractant and Can Self-Organize to Form Clusters

The process of organized cell migration involves many spatially regulated events, the first of which is sensing a gradient (Iglesias and Devreotes, 2008). WNT5A, a PCP ligand, establishes PCP

(I) Quantification of the number of normal villi per 100 μ m in control and *Fat4-Dchs1* mutant proximal intestines (reported as mean \pm SEM; *p < 0.05, **p < 0.005; n = 3).

(J) Quantification of the number of PDGFR α + clusters per 100 μ m in control and *Fat4-Dchs1* mutant proximal intestines (reported as mean \pm SEM; *p < 0.05, **p < 0.005, ***p < 0.0005; n = 3).

(K) Quantified widths of villus fusions relative to the widths of normal villi in proximal intestines of *Fat4-Dchs1* mutants (reported as mean \pm SEM; *p < 0.05, **p < 0.005; n = 3). Representative normal villi and fused villi are outlined in dotted lines in all H&E and immunostained images.

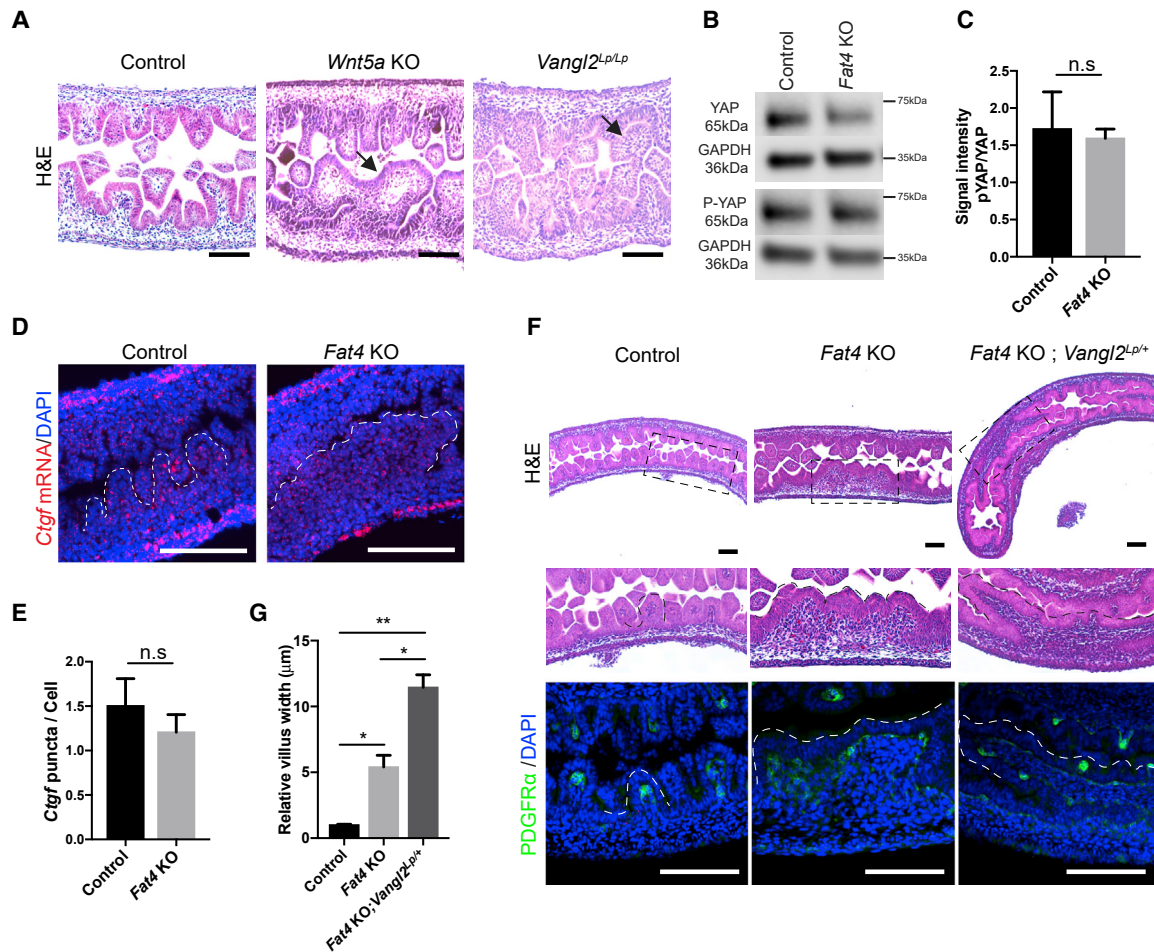


Figure 3. Core PCP Pathway Is Required for Villification and Acts in Parallel to the *Fat4*-*Dchs1* Axis

(A) Representative H&E analysis of control, *Wnt5a* KO, and *Vangl2*^{Lp/Lp} mutant intestines at E15.5. Fused villus areas are denoted by the arrows.

(B) Representative western blot of YAP (top panel) and phospho-YAP (P-YAP) (lower panel) with loading control GAPDH of control and *Fat4* KO E15.5 intestinal protein lysates. See Figure S4 for full blot.

(C) Quantification of GAPDH normalized signal intensities of P-YAP and YAP western blots from Figure 3B. P-YAP and YAP levels in control and *Fat4* KO mutants show no significant differences (reported as mean ± SEM; n.s., not significant; n = 3).

(D) Representative images of smFISH for the YAP target gene *Ctgf* in controls and *Fat4* KOs. See Figure S3A for controls. White dotted lines outline the villi in control and villus fusion in mutant images.

(E) Quantification of *Ctgf* transcripts per DAPI+ cell from smFISH analysis shows no significant difference between controls and *Fat4* KOs (reported as mean ± SEM; n.s., not significant; n = 3).

(F) Representative histological analysis of control, *Fat4* KO, and *Fat4* KO;*Vangl2*^{Lp/+} mutants. H&E images show a more severe villus fusion in *Fat4* KO;*Vangl2*^{Lp/+} mutants compared to *Fat4* KO. Regions within the black box are magnified in the panel below. Immunofluorescence staining with PDGFRα shows disrupted mesenchymal clustering in the large fusion area of *Fat4* KO;*Vangl2*^{Lp/+} mutants. *Fat4* KO images are of a different biological replicate than shown in Figures 2B and 2C.

(G) Quantification of fused villus width relative to normal villus width in proximal intestines indicates a significantly larger villus fusion width in *Fat4* KO;*Vangl2*^{Lp/+} than *Fat4* KO alone (represented as mean ± SEM; *p < 0.05, **p < 0.005; n = 3). Villus width values from control and *Fat4* KO were taken from Figure 2K and used in this figure to compare to the *Fat4* KO;*Vangl2*^{Lp/+} dataset. Dotted lines outline normal and fused villi in controls and mutants, respectively. All scale bars, 100 μm.

gradients along the P-D axis of the developing limb buds (Gao et al., 2011) and can act as a chemoattractant for mouse palate mesenchymal cells (Witze et al., 2008). Since PDGFRα+ cells exhibit directional cell migration, we asked whether WNT5A could serve as a chemoattractant during mesenchymal clustering. SmFISH of *Wnt5a* transcript in wild-type intestines revealed high levels at the villus core, consistent with graded expression ascending toward stromal clustering cells (Figure 6A). This graded *Wnt5a* expression along the villus is maintained

throughout late development (Gregorieff et al., 2005). To determine whether PDGFRα+ cells can migrate in response to exogenous WNT5A, we isolated GFP+ cells from *Pdgfra*^{H2B-eGFP} mice through fluorescence-activated cell sorting and subjected them to *in vitro* transwell migration assays with a WNT5A chemo-gradient (Figures 6B–6D, S5A, and S5B). PDGFRα GFP+ cells from control mice significantly migrated toward the WNT5A source, indicating a chemoattractant response (Figures 6C and 6D). However, *Fat4* KO PDGFRα+ cells showed no

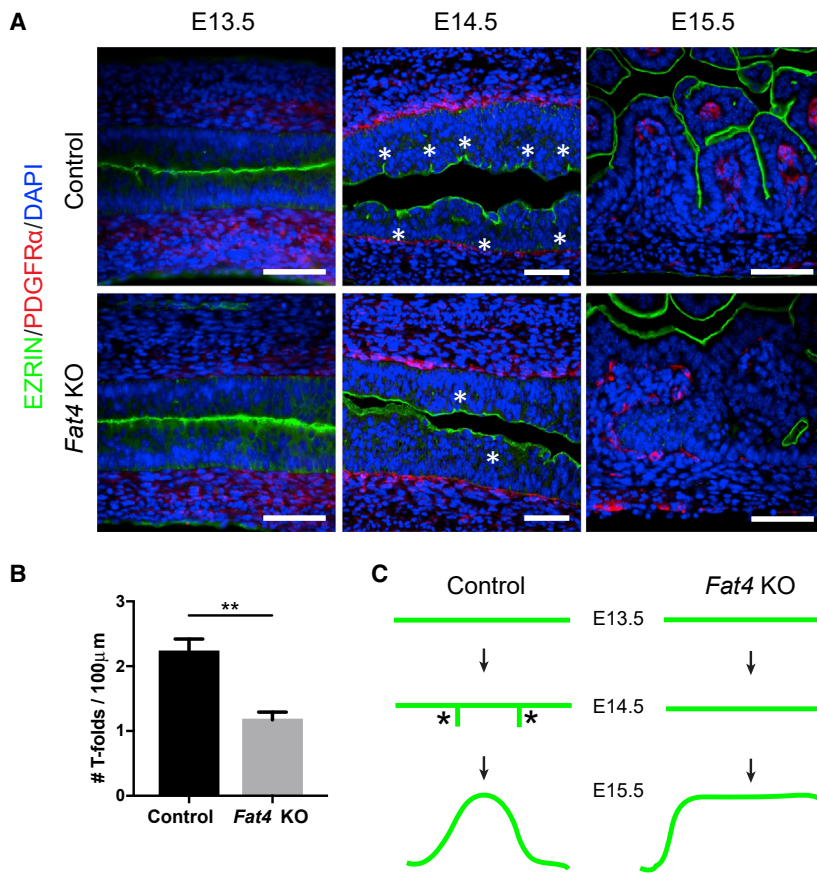


Figure 4. *Fat4*-PCP in the Stroma Demarcates Villus Boundaries for Epithelial Remodeling

(A) Representative images of immunofluorescence-stained control and *Fat4* KO intestines before (E13.5), during (E14.5), and after (E15.5) the onset of villification with apical membrane marker, EZRIN, and stromal cluster marker, PDGFR α . T-folds appeared at E14.5 (denoted with asterisks). At E15.5, the villus fusion was seen in the *Fat4* KOs with a lack of villus boundary visualized by EZRIN. (B) Quantification of T-folding at E14.5 shows significantly fewer number of T-folds in *Fat4* KOs than controls (reported as mean \pm SEM, ** $p < 0.005$, $n = 5$).

(C) Model of villus fusion phenotype due to a lack of villus boundaries. Green line represents the apical membrane. In controls, mesenchymal clustering initiates epithelial T-folding (asterisks), resulting in villus emergence. In the *Fat4* KO, mesenchymal clustering and T-folding fail to occur, leading to the lack of villus boundaries with villus fusion. Scale bars, 100 μ m.

difference in migration despite the addition of WNT5A (Figures 6C and 6D). These findings reveal WNT5A as a critical chemoattractant for PDGFR α + stromal cell migration during villification, upstream of *Fat4*.

Since PDGFR α + mesenchymal cells express a high level of *Wnt5a*, we hypothesized that these cells exhibit a unique clustering behavior even in the absence of chemoattractant signals. We modeled cluster formation *in vitro* by employing three-dimensional (3D) culture systems. Indeed, 5 days after plating PDGFR α GFP+ cells in Matrigel supplemented with culture media, the cells self-organized to form 3D spheroids, resembling *in vivo* mesenchymal clusters (Figure 6E). Notably, this clustering ability was significantly impaired in PDGFR α + cells isolated from *Fat4* KO mice, which formed fewer and smaller spheroids, revealing a critical role for *Fat4*-PCP in self-organization (Figures 6E and 6F). To determine if self-organization is unique to PDGFR α + mesenchymal cells, we cultured PDGFR α GFP-EPCAM- cells and found that this population could not form spheroids (Figures 6G and S5C). Therefore, self-organization for cluster formation represents a unique and intrinsic property of PDGFR α + mesenchymal cells. To check whether spheroid formation reflected cell migration rather than proliferation, we immunostained the structures for the proliferation marker PCNA. As the spheroids were negative for PCNA, they were most likely formed because of cell migration rather than proliferation (Figures 6H, S6A, and S6B). To investigate further a functional link between Hh signaling and its downstream PCP

pathway, we treated PDGFR α GFP+ cells from control E15.5 embryos with cyclopamine, a Hh antagonist, and performed a transwell migration assay as a proxy for PCP function. Cyclopamine-treated cells migrated significantly less than vehicle-treated cells in the presence of WNT5A chemoattractant, demonstrating functional evidence for Hh regulation of

PCP-mediated migration (Figure S6C). We next asked whether overexpression of PCP can restore these cell migration defects. Indeed, *FAT4* and *DCHS1*-transfected PDGFR α + cells confers a significant rescue to cell migration ability compared to empty vector controls in the presence of cyclopamine (Figures 6I, 6J, and S6D). Taken together, these results demonstrate that PCP regulates the organized stromal cell clustering behavior required for villification in response to Hh signaling activation.

DISCUSSION

Key developmental pathways are known to play critical roles during morphogenesis, but how these patterning signals coordinate with cellular movements to achieve specific morphogenesis remains poorly understood. Our study reveals Hh-activated mesenchymal PCP as a key regulator required for oriented cell movements in intestinal villification. Gut mesenchymal Hh signaling is known to be necessary for stromal maintenance and muscle differentiation (Huang et al., 2013; Mao et al., 2010; Ramalho-Santos et al., 2000), and we now show that it also directly regulates mesenchymal cell clustering by activating cell adhesion and PCP genes. These findings provide new mechanistic insight into villus formation.

Drosophila studies originally described PCP as the orientation of cells perpendicular to the apical-basal axis of an epithelial sheet, as PCP seemed to be restricted to either flat epithelia such as the wing and eye (Yang and Mlodzik, 2015) or motile

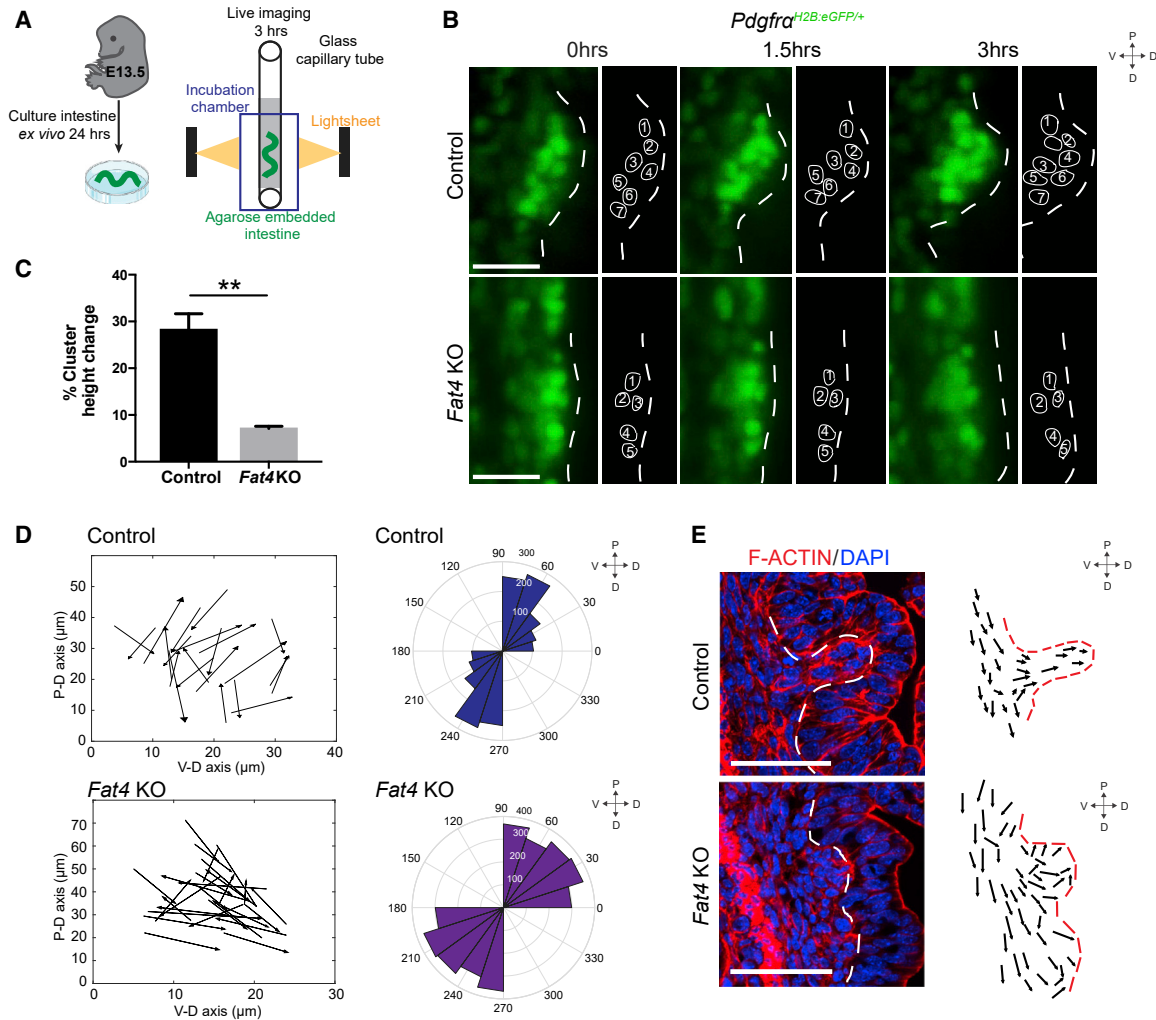


Figure 5. *Fat4*-PCP Directs Stromal Migration and Cell Orientation for Clustering Behavior during Villification

(A) Schematic representation of live-imaging setup. *Pdgfra*^{H2B:eGFP/+} control and *Fat4* KO intestines were dissected at E13.5, cultured *ex vivo* for 24 h, and then suspended in an agarose gel inside a glass capillary tube for light-sheet imaging in an incubation chamber.

(B) Representative images of live-imaging movies (Videos S1 and S2) of *Pdgfra*^{H2B:eGFP/+} intestines versus *Pdgfra*^{H2B:eGFP/+}; *Fat4* KO mutants. Each cell is labeled with a number and positions were tracked over 3 h (shown adjacent to image). In control intestines, the formation of GFP+ mesenchymal clusters were observed. In *Fat4* KO intestines, GFP+ cells failed to form clusters in some regions. The dotted lines outline the protruding mesenchyme as clustering occurs, in the apical direction.

(C) Quantification of % cluster height change over time. *Fat4* KO mutants exhibited significantly decreased cluster height change compared to controls (reported as mean \pm SEM, ***p* < 0.005, *n* = 3). (D) Visualization and quantification of PDGFR α GFP+ cell movement (position change over time) from live images (Videos S1 and S2). Left panel shows GFP+ cell movement over time, where each arrow represents a cell (the tail represents the start position (0 h), while the arrowhead represents the end position (3 h)). The right panel shows cell tracking data as directional displacements presented as a rose plot. In control intestines, GFP+ cell movement occurred predominantly along the P-D axis. In *Fat4* KO intestines, GFP+ cell movement was disorganized, lacking a specific direction (*n* = 3).

(E) Representative immunofluorescence-stained control and *Fat4* KO intestines at E15.5 to visualize F-actin by phalloidin. Using DAPI (nuclear) and F-actin (membrane) staining, stromal cell orientations beneath emerging villus in controls and *Fat4* KOs were drawn (right panel). Arrows denote the orientation of cells (along the longest axis of the cell). Control stromal cells at the villus core were oriented toward the D-V axis, whereas closer to the muscle layer, they were oriented along the P-D axis. *Fat4* KO stromal cells lacked organized orientation at the villus core (*n* = 3). Scale bars, 50 μ m.

epithelial border cells for collective migration during development (Bastock and Strutt, 2007). However, vertebrate studies indicate that stromal PCP also plays a critical role in proper organization of physically complex tissues such as the limb bud (Gao et al., 2011). Our results reveal the significance of Hh-mediated mesenchymal PCP in mammalian intestinal morphogenesis.

Villus fusion is not commonly observed in animal studies. At E15.5, fusions in most of the PCP mutants we studied (*Fat4*, *Dchs1*, *Vangl2*, and *Wnt5a*) were largely confined to the proximal duodenum, with the exception of *Fat4*^{-/-}; *Vangl2*^{LP/+} mutants, where the fusion spanned much of the duodenum. The latter mutant reveals partial redundancy of *Fat4* and *Vangl2* signaling axes but regionally restricted villus fusion implies that

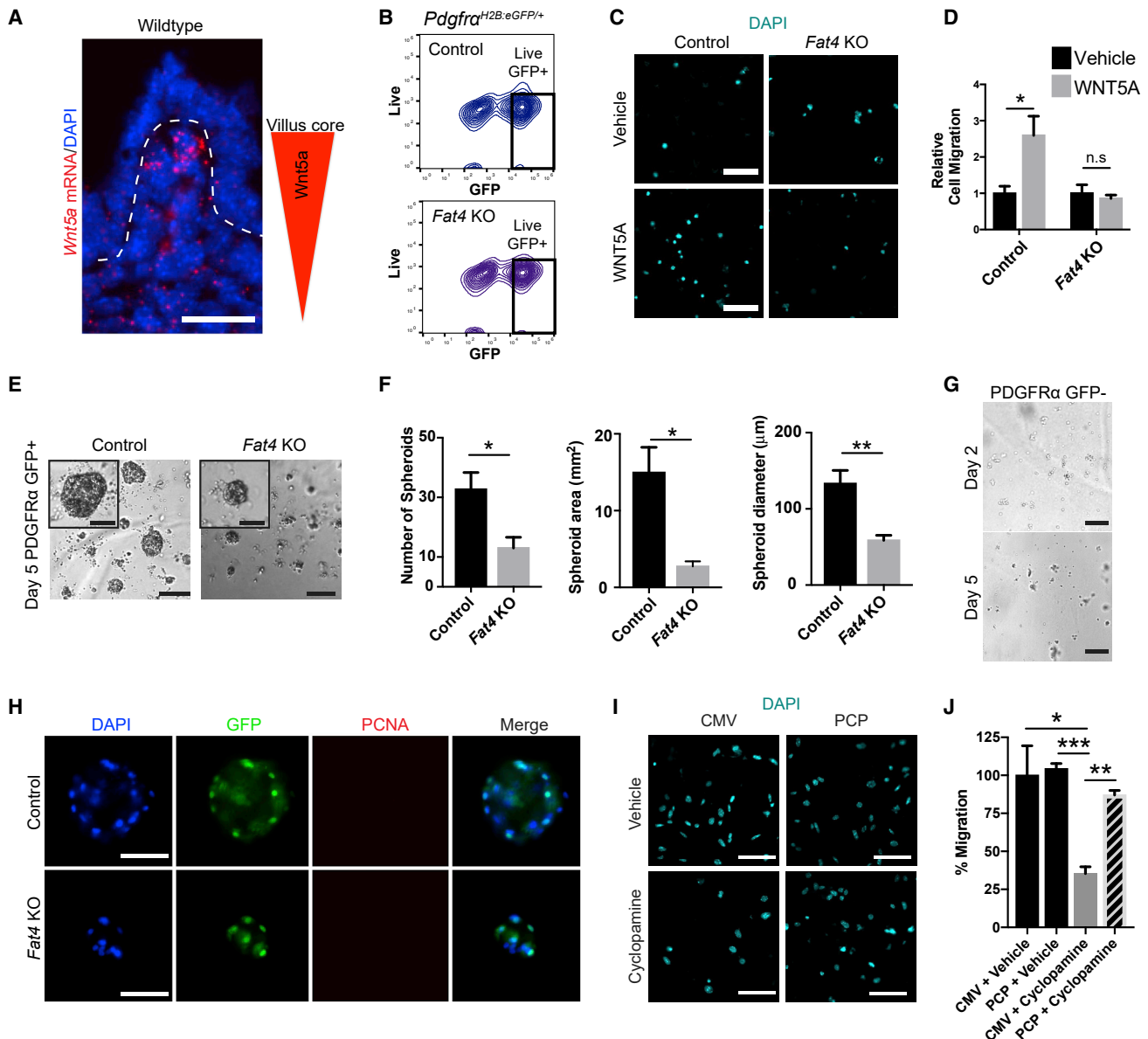


Figure 6. PDGFR α + Clustering Cells Respond to WNT5A as a Chemoattractant and Require Fat4-PCP for Self-Organization

(A) SmFISH for *Wnt5a* transcript in wild-type intestines at E15.5 showed graded expression in the lamina propria, highest at the villus core ($n = 3$). White dotted line indicates the epithelial-mesenchymal border. Scale bar is 25 μm .

(B) Sorting scheme from *Pdgfra*^{H2B:eGFP/+} (control) and *Pdgfra*^{H2B:eGFP/+}; *Fat4* KO intestines at E15.5 for live (Sytox Blue⁻) GFP+ populations. Refer to Figures S5A and S5B for full sorting scheme.

(C) Transwell migration assays for PDGFR α GFP+ cell migration guided by WNT5A. Control GFP+ cells migrated in response to WNT5A compared to BSA vehicle treatment. *Fat4* KO GFP+ cells failed to migrate in response to WNT5A. Scale bars, 50 μm .

(D) Quantification of cell migration in response to WNT5A relative to BSA vehicle treatment from (C). Controls showed a significant increase in migration upon WNT5A addition. *Fat4* KO cells displayed no significant difference in migration with WNT5A (reported as mean \pm SEM; * $p < 0.05$; n.s., not significant; $n = 3$).

(E) Representative images of spheroid formation at day 5 of GFP+ cells isolated from *Pdgfra*^{H2B:eGFP/+} controls and *Pdgfra*^{H2B:eGFP/+}; *Fat4* KO mutants plated in 3D culture conditions. Insets are of higher magnification to visualize the size differences of a single spheroid. Scale bars, 120 and 60 μm (inset).

(F) Quantification of spheroid formation shows a significant decrease in the number (left plot) and size (center and right plot) of spheroids derived from *Fat4* KO cells compared to controls (reported as mean \pm SEM; ** $p < 0.005$, * $p < 0.05$; $n = 6-7$).

(G) PDGFR α GFP-EPCAM- stromal cells from *Pdgfra*^{H2B:eGFP/+} controls failed to self-organize into spheroids *in vitro* ($n = 3$). Refer to Figure S5C for full sorting scheme. Scale bars, 120 μm .

(H) Representative images of immunofluorescence-stained control and *Fat* KO spheroids with PCNA at day 5 show a lack of proliferative cells. See Figure S6A for time course PCNA stain. Scale bars, 60 μm .

(legend continued on next page)

mechanisms beyond PCP also contribute to mesenchymal clustering. Future examination of other cell polarity genes and pathways will inform our understanding on this point.

Two different models exist to explain villus morphogenesis. One model suggests that a physical constriction from differentiating smooth muscle in the mesenchyme applies sufficient force for the overlying epithelium to buckle and form outward villus projections (Shyer et al., 2013). The second model proposes that tightly controlled cell-cell signaling between the epithelium and its underlying mesenchyme induces mesenchymal clustering, patterned in a Turing-like manner and subsequently leading to epithelial remodeling (Walton et al., 2012, 2016b). Our work demonstrates that Hh- and GLI2-mediated activation of atypical cadherin and PCP genes is critical for mouse mesenchymal clustering and villification. Atypical cadherin and PCP mutant mice showed no obvious defects in muscle differentiation, further supporting a central role for mesenchymal clustering in villification. Of note, distinct morphogenetic events underlie avian and mammalian villus formation: chick epithelia undergo progressive folding to form ridges followed by zigzag bending, which leads subsequently to villus formation, and this process indeed coincides with muscle differentiation (Shyer et al., 2013). In contrast, mammalian villification involves the direct emergence of villus-like dome structures from the flat epithelium, without ridge and zigzag formation. These studies thus highlight likely divergent evolutionary mechanisms. It will be instructive to investigate human villus formation to confirm this proposed role of mesenchymal clustering in mammals.

Although mouse tissues are less amenable to live microscopy than other model organisms, we utilized live light-sheet microscopy to image the embryonic mouse intestine *ex vivo* for extended periods of time (over 3 h) with appropriate depth and minimal photo-toxicity. We thus captured mesenchymal clustering behavior and revealed altered cell movement in *Fat4* mutants. This approach could be extended to study human villification. Of note, patients with celiac disease commonly suffer from malnutrition due to villus atrophy, as apoptosis of enterocytes results in a flattened epithelium with markedly reduced surface area (Corazza et al., 1997). A better understanding of mesenchymal PCP mechanisms in human villification could form a basis for new therapies that promote villus regeneration.

STAR★METHODS

Detailed methods are provided in the online version of this paper and include the following:

- KEY RESOURCES TABLE
- LEAD CONTACT AND MATERIALS AVAILABILITY
- EXPERIMENTAL MODEL AND SUBJECT DETAILS
 - Animals
 - Cell Lines
- METHOD DETAILS

- RNA-seq and ChIP-seq
- Electron Microscopy, Histology and Immunostaining
- RNA Quantification and Visualization
- Cell Isolation and Sorting
- Live Imaging
- *In Vitro* Assays
- QUANTIFICATION AND STATISTICAL ANALYSIS
- DATA AND CODE AVAILABILITY

SUPPLEMENTAL INFORMATION

Supplemental Information can be found online at <https://doi.org/10.1016/j.devcel.2020.02.003>.

ACKNOWLEDGMENTS

This work was supported by SickKids Foundation start-up, the Natural Sciences and Engineering Research Council of Canada (NSERC) Discovery #RGPIN-2016-06093 grant, and the March of Dimes Basil O'Connor Starter Scholar Research Award (T.-H.K.); the SickKids Restrucamp and Ontario Graduate Scholarships (A.R.-B.); the grants U.S. NSF IOS-1257540 and U.S. NIH HD083625 (A.L.); NSERC Discovery and the Canadian Institutes of Health Research grants (C.-C.H.); NIH grant R01DK081113 (R.A.S.); and Canadian Institutes of Health Research (CIHR) foundation grant (H.M., a BJC investigator and a Larry J. and Carol A. Shapiro Professor at Washington University School of Medicine). We thank Dr. Warren Zimmer for *Bapx1^{Cre}* mice, Dr. Philippe Gros for VANGL2 antibodies, and Edward Espinoza for helpful discussion.

AUTHOR CONTRIBUTIONS

A.R.-B. designed and performed the experiments, analyzed the data, and wrote the manuscript; M.Z. performed and analyzed the live-imaging data; W.-C.Y. performed the ChIP-seq and analyzed the data; S.C. performed the RNA-seq and ChIP-seq; X.Z. helped with the ChIP-seq validation studies; J.W. helped with the cell culture studies; Y.S. supervised the imaging analysis; C.H.D. provided the PCP mutant embryos; A.L. provided the PCP mutant embryos; C.-C.H. provided the Hh mutant mice and supervised the bioinformatic analyses of ChIP-seq and RNA-seq; R.A.S. supervised the initiation of this project; H.M. provided the *Fat4*, *Dchs1*, and *Vangl2* mutant mice and helpful suggestions; S.H. supervised the imaging analysis; and T.-H.K. conceived and supervised the study, analyzed the data, and wrote the manuscript.

DECLARATION OF INTERESTS

The authors declare no competing interests.

Received: January 14, 2019

Revised: November 6, 2019

Accepted: February 3, 2020

Published: March 9, 2020

REFERENCES

- Barnett, D.W., Garrison, E.K., Quinlan, A.R., Strömberg, M.P., and Marth, G.T. (2011). BamTools: a C++ API and toolkit for analyzing and managing BAM files. *Bioinformatics* 27, 1691–1692.
- Bastock, R., and Strutt, D. (2007). The planar polarity pathway promotes coordinated cell migration during *Drosophila* oogenesis. *Development* 134, 3055–3064.

(I) Representative images of transfected PDGFR α GFP+ cell migration upon treatment with cyclopamine in a transwell migration assay with WNT5A. Cells were transfected with either empty (CMV) or *FAT4* and *DCHS1* (PCP) overexpression vectors and treated with either vehicle control or cyclopamine at 5 μ M. Scale bars, 50 μ m.

(J) Quantification of the percentage of cell migration relative to empty vector vehicle control (at 100%) shows a significant decrease in migration upon cyclopamine treatment and rescue of cell migration upon PCP transfection (reported as mean \pm SEM; * p < 0.05, ** p < 0.005, *** p < 0.0005; n = 3).

- Blair, S., and McNeill, H. (2018). Big roles for Fat cadherins. *Curr. Opin. Cell Biol.* *51*, 73–80.
- Bolger, A.M., Lohse, M., and Usadel, B. (2014). Trimmomatic: a flexible trimmer for Illumina sequence data. *Bioinformatics* *30*, 2114–2120.
- Bray, N.L., Pimentel, H., Melsted, P., and Pachter, L. (2016). Near-optimal probabilistic RNA-seq quantification. *Nat. Biotechnol.* *34*, 525–527.
- Briscoe, J., and Théron, P.P. (2013). The mechanisms of Hedgehog signalling and its roles in development and disease. *Nat. Rev. Mol. Cell Biol.* *14*, 416–429.
- Cappello, S., Gray, M.J., Badouel, C., Lange, S., Einsiedler, M., Srour, M., Chitayat, D., Hamdan, F.F., Jenkins, Z.A., Morgan, T., et al. (2013). Mutations in genes encoding the cadherin receptor-ligand pair DCHS1 and FAT4 disrupt cerebral cortical development. *Nat. Genet.* *45*, 1300–1308.
- Cervantes, S., Yamaguchi, T.P., and Hebrok, M. (2009). Wnt5a is essential for intestinal elongation in mice. *Dev. Biol.* *326*, 285–294.
- Cheung, H.O., Zhang, X., Ribeiro, A., Mo, R., Makino, S., Puvion-Randall, V., Law, K.K., Briscoe, J., and Hui, C.C. (2009). The kinesin protein Kif7 is a critical regulator of Gli transcription factors in mammalian hedgehog signaling. *Sci. Signal.* *2*, ra29.
- Coquenlorge, S., Yin, W.C., Yung, T., Pan, J., Zhang, X., Mo, R., Belik, J., Hui, C.C., and Kim, T.H. (2019). GLI2 modulated by SUFU and SPOP induces intestinal stem cell niche signals in development and tumorigenesis. *Cell Rep* *27*, 3006–3018.e4.
- Corazza, G.R., Biagi, F., Volta, U., Andreani, M.L., De Franceschi, L., and Gasbarrini, G. (1997). Autoimmune enteropathy and villous atrophy in adults. *Lancet* *350*, 106–109.
- Ding, Q., Fukami, S., Meng, X., Nishizaki, Y., Zhang, X., Sasaki, H., Dlugosz, A., Nakafuku, M., and Hui, C.C. (1999). Mouse suppressor of fused is a negative regulator of sonic hedgehog signaling and alters the subcellular distribution of Gli1. *Curr. Biol.* *9*, 1119–1122.
- Freddo, A.M., Shoffner, S.K., Shao, Y., Taniguchi, K., Grosse, A.S., Guysinger, M.N., Wang, S., Rudraraju, S., Margolis, B., Garikipati, K., et al. (2016). Coordination of signaling and tissue mechanics during morphogenesis of murine intestinal villi: a role for mitotic cell rounding. *Integr Biol (Camb)* *8*, 918–928.
- Gao, B., Song, H., Bishop, K., Elliot, G., Garrett, L., English, M.A., Andre, P., Robinson, J., Sood, R., Minami, Y., et al. (2011). Wnt signaling gradients establish planar cell polarity by inducing Vangl2 phosphorylation through Ror2. *Dev. Cell* *20*, 163–176.
- Gregorieff, A., Pinto, D., Begthel, H., Destrée, O., Kielman, M., and Clevers, H. (2005). Expression pattern of Wnt signaling components in the adult intestine. *Gastroenterology* *129*, 626–638.
- Hamilton, T.G., Klinghoffer, R.A., Corrin, P.D., and Soriano, P. (2003). Evolutionary divergence of platelet-derived growth factor alpha receptor signaling mechanisms. *Mol. Cell. Biol.* *23*, 4013–4025.
- Huang, H., Cotton, J.L., Wang, Y., Rajurkar, M., Zhu, L.J., Lewis, B.C., and Mao, J. (2013). Specific requirement of Gli transcription factors in Hedgehog-mediated intestinal development. *J. Biol. Chem.* *288*, 17589–17596.
- Iglesias, P.A., and Devreotes, P.N. (2008). Navigating through models of chemotaxis. *Curr. Opin. Cell Biol.* *20*, 35–40.
- Kamachi, Y., and Kondoh, H. (1993). Overlapping positive and negative regulatory elements determine lens-specific activity of the delta 1-crystallin enhancer. *Mol. Cell. Biol.* *13*, 5206–5215.
- Karlsson, L., Lindahl, P., Heath, J.K., and Betsholtz, C. (2000). Abnormal gastrointestinal development in PDGF-A and PDGFR- α deficient mice implicates a novel mesenchymal structure with putative instructive properties in villus morphogenesis. *Development* *127*, 3457–3466.
- Le Guen, L., Marchal, S., Faure, S., and de Santa Barbara, P. (2015). Mesenchymal-epithelial interactions during digestive tract development and epithelial stem cell regeneration. *Cell. Mol. Life Sci.* *72*, 3883–3896.
- Leung, V., Iliescu, A., Jolicoeur, C., Gravel, M., Apuzzo, S., Torban, E., Cayouette, M., and Gros, P. (2016). The planar cell polarity protein Vangl2 is required for retinal axon guidance. *Dev. Neurobiol.* *76*, 150–165.
- Li, H., and Durbin, R. (2009). Fast and accurate short read alignment with Burrows-Wheeler transform. *Bioinformatics* *25*, 1754–1760.
- Li, Z.J., Nieuwenhuis, E., Nien, W., Zhang, X., Zhang, J., Puvion-Randall, V., Wainwright, B.J., Kim, P.C., and Hui, C.C. (2012). Kif7 regulates Gli2 through SuFu-dependent and -independent functions during skin development and tumorigenesis. *Development* *139*, 4152–4161.
- Love, M.I., Huber, W., and Anders, S. (2014). Moderated estimation of fold change and dispersion for RNA-seq data with DESeq2. *Genome Biol* *15*, 550.
- Loza, O., Heemskerk, I., Gordon-Bar, N., Amir-Zilberstein, L., Jung, Y., and Sprinzak, D. (2017). A synthetic planar cell polarity system reveals localized feedback on Fat4-Ds1 complexes. *Elife* *6*, e24820.
- Mao, J., Kim, B.M., Rajurkar, M., Shivdasani, R.A., and McMahon, A.P. (2010). Hedgehog signaling controls mesenchymal growth in the developing mammalian digestive tract. *Development* *137*, 1721–1729.
- Mao, Y., Kuta, A., Crespo-Enriquez, I., Whiting, D., Martin, T., Mulvaney, J., Irvine, K.D., and Francis-West, P. (2016). Dchs1-Fat4 regulation of polarized cell behaviours during skeletal morphogenesis. *Nat. Commun.* *7*, 11469.
- Mao, Y., Mulvaney, J., Zakaria, S., Yu, T., Morgan, K.M., Allen, S., Basson, M.A., Francis-West, P., and Irvine, K.D. (2011). Characterization of a Dchs1 mutant mouse reveals requirements for Dchs1-Fat4 signaling during mammalian development. *Development* *138*, 947–957.
- Mi, H., Huang, X., Muruganujan, A., Tang, H., Mills, C., Kang, D., and Thomas, P.D. (2017). PANTHER version 11: expanded annotation data from Gene Ontology and Reactome pathways, and data analysis tool enhancements. *Nucleic Acids Res* *45*, D183–D189.
- Mi, H., Muruganujan, A., Casagrande, J.T., and Thomas, P.D. (2013). Large-scale gene function analysis with the PANTHER classification system. *Nat. Protoc.* *8*, 1551–1566.
- Mi, H., Muruganujan, A., Huang, X., Ebert, D., Mills, C., Guo, X., and Thomas, P.D. (2019). Protocol update for large-scale genome and gene function analysis with the PANTHER classification system (v.14.0). *Nat. Protoc.* *14*, 703–721.
- Montcouquiol, M., Rachel, R.A., Lanford, P.J., Copeland, N.G., Jenkins, N.A., and Kelley, M.W. (2003). Identification of Vangl2 and Scrb1 as planar polarity genes in mammals. *Nature* *423*, 173–177.
- Quinlan, A.R., and Hall, I.M. (2010). BEDTools: a flexible suite of utilities for comparing genomic features. *Bioinformatics* *26*, 841–842.
- Ragni, C.V., Diguët, N., Le Garrec, J.F., Novotova, M., Resende, T.P., Pop, S., Charon, N., Guillemot, L., Kitasato, L., Badouel, C., et al. (2017). Amotl1 mediates sequestration of the Hippo effector Yap1 downstream of Fat4 to restrict heart growth. *Nat. Commun.* *8*, 14582.
- Ramalho-Santos, M., Melton, D.A., and McMahon, A.P. (2000). Hedgehog signals regulate multiple aspects of gastrointestinal development. *Development* *127*, 2763–2772.
- Saburi, S., Hester, I., Fischer, E., Pontoglio, M., Eremina, V., Gessler, M., Quaggin, S.E., Harrison, R., Mount, R., and McNeill, H. (2008). Loss of Fat4 disrupts PCP signaling and oriented cell division and leads to cystic kidney disease. *Nat. Genet.* *40*, 1010–1015.
- Schmidt, D., Wilson, M.D., Spyrou, C., Brown, G.D., Hadfield, J., and Odom, D.T. (2009). ChIP-seq: using high-throughput sequencing to discover protein-DNA interactions. *Methods* *48*, 240–248.
- Shyer, A.E., Tallinen, T., Nerurkar, N.L., Wei, Z., Gil, E.S., Kaplan, D.L., Tabin, C.J., and Mahadevan, L. (2013). Villification: how the gut gets its villi. *Science* *342*, 212–218.
- Soneson, C., Love, M.I., and Robinson, M.D. (2015). Differential analyses for RNA-seq: transcript-level estimates improve gene-level inferences. *F1000Res.* *4*, 1521.
- Supek, F., Bošnjak, M., Škunca, N., and Šmuc, T. (2011). REVIGO summarizes and visualizes long lists of gene ontology terms. *PLoS One* *6*, e21800.
- Verzi, M.P., Stanfel, M.N., Moses, K.A., Kim, B.M., Zhang, Y., Schwartz, R.J., Shivdasani, R.A., and Zimmer, W.E. (2009). Role of the homeodomain transcription factor Bapx1 in mouse distal stomach development. *Gastroenterology* *136*, 1701–1710.
- Walton, K.D., Freddo, A.M., Wang, S., and Gumucio, D.L. (2016a). Generation of intestinal surface: an absorbing tale. *Development* *143*, 2261–2272.

- Walton, K.D., Kolterud, A., Czerwinski, M.J., Bell, M.J., Prakash, A., Kushwaha, J., Grosse, A.S., Schnell, S., and Gumucio, D.L. (2012). Hedgehog-responsive mesenchymal clusters direct patterning and emergence of intestinal villi. *Proc. Natl. Acad. Sci. USA* *109*, 15817–15822.
- Walton, K.D., Whidden, M., Kolterud, Å., Shoffner, S.K., Czerwinski, M.J., Kushwaha, J., Parmar, N., Chandrasekhar, D., Freddo, A.M., Schnell, S., and Gumucio, D.L. (2016b). Villification in the mouse: Bmp signals control intestinal villus patterning. *Development* *143*, 427–436.
- Wang, C., Pan, Y., and Wang, B. (2010). Suppressor of fused and Spop regulate the stability, processing and function of Gli2 and Gli3 full-length activators but not their repressors. *Development* *137*, 2001–2009.
- Witze, E.S., Litman, E.S., Argast, G.M., Moon, R.T., and Ahn, N.G. (2008). Wnt5a control of cell polarity and directional movement by polarized redistribution of adhesion receptors. *Science* *320*, 365–369.
- Yang, Y., and Mlodzik, M. (2015). Wnt-Frizzled/planar cell polarity signaling: cellular orientation by facing the wind (Wnt). *Annu. Rev. Cell Dev. Biol.* *31*, 623–646.
- Zhang, Y., Liu, T., Meyer, C.A., Eeckhoute, J., Johnson, D.S., Bernstein, B.E., Nusbaum, C., Myers, R.M., Brown, M., Li, W., Liu, X.S., et al. (2008). Model-based analysis of ChIP-Seq (MACS). *Genome Biol.* *9*, R137.
- Zhao, B., Ye, X., Yu, J., Li, L., Li, W., Li, S., Yu, J., Lin, J.D., Wang, C.Y., Chinnaiyan, A.M., et al. (2008). TEAD mediates YAP-dependent gene induction and growth control. *Genes Dev.* *22*, 1962–1971.

STAR★METHODS

KEY RESOURCES TABLE

REAGENT or RESOURCE	SOURCE	IDENTIFIER
Antibodies		
Rabbit anti-GLI2	Cheung et al., 2009	
Mouse anti-H3K27Ac	Millipore	Cat# 05-1334; RRID: AB_1977244
Rabbit anti-PDGFRalpha C-20S	Santa Cruz Biotechnology	Cat# sc-338; RRID: AB_631064
Rabbit anti-YAP (D8H1X) XP	Cell Signaling Technology	Cat# 14074; RRID: AB_2650491
Rabbit anti-Phospho-YAP (Ser127)	Cell Signaling Technology	Cat# 4911; RRID: AB_2218913
Rabbit anti-GAPDH [EPR16891]	Abcam	Cat# ab181602; RRID: AB_2630358
Mouse anti-EZRIN	Sigma-Aldrich	Cat# E8897; RRID: AB_476955
Mouse anti-PCNA	Santa Cruz Technology	Cat# sc-56; RRID: AB_628110
Mouse anti-alpha smooth muscle Actin	Abcam	Cat# ab7817; RRID: AB_262054
Rabbit anti-alpha smooth muscle Actin	Abcam	Cat# ab124964; RRID: AB_11129103
Rabbit anti-SM22	Abcam	Cat# ab14106; RRID: AB_443021
Rabbit anti-H3K27me3	Millipore	Cat# 07-449; RRID: AB_310624
EpCAM antibody (G8.8) (Allophycocyanin)	Abcam	Cat# ab95641; RRID: AB_10677416
Rabbit anti-VANGL2	Gift from Dr. Philippe Gros (Leung et al., 2016)	N/A
Goat anti-Mouse IgG Secondary (Alexa Fluor 568)	Thermo Fisher Scientific	Cat# A-11031; RRID: AB_144696
Goat anti-Mouse IgG Secondary (Alexa Fluor 488)	Thermo Fisher Scientific	Cat# A-11029; RRID: AB_2534088
Goat anti-Rabbit IgG Secondary (Alexa Fluor 488)	Thermo Fisher Scientific	Cat# A-11034; RRID: AB_2576217
Goat anti-Rabbit IgG Secondary (Alexa Fluor 568)	Thermo Fisher Scientific	Cat# A-11036; RRID: AB_10563566
Goat anti-Rabbit IgG Secondary (HRP)	Thermo Fisher Scientific	Cat# 31460; RRID: AB_228341
Chemicals, Peptides, and Recombinant Proteins		
32% Paraformaldehyde	Electron Microscopy Sciences	Cat# 15714
Harris' Hematoxylin	Electron Microscopy Sciences	Cat # 26041-06
Alcoholic Eosin Y	Electron Microscopy Sciences	Cat# 26051-11
Alexa Fluor 568 Phalloidin	Thermo Fisher Scientific	Cat# A12380
Recombinant Human/Mouse Wnt-5a Protein	R&D Systems	Cat# 645-WN-010
Cyclopamine	Toronto Research Chemicals	Cat# C988400
Critical Commercial Assays		
Dual Luciferase Reporter Assay System	Promega	Cat# E1910
Pierce BCA Protein Assay Kit	Thermo Fisher Scientific	Cat# 23225
SuperSignal West Femto Maximum Sensitivity Substrate Kit	Thermo Fisher Scientific	Cat# 34095
RNAscope Multiplex Fluorescent v2 Kit	Advanced Cell Diagnostics	Cat# 323100
Deposited Data		
GEO accession for RNA-Seq	Coquenlorge et al., 2019	GEO: GSE103683
GEO accession for ChIP-Seq	Coquenlorge et al., 2019	GEO: GSE103690
Experimental Models: Cell Lines		
C3H10T1/2 mouse embryonic fibroblast cells	ATCC	ATCC CCL-226

(Continued on next page)

Continued

REAGENT or RESOURCE	SOURCE	IDENTIFIER
Experimental Models: Organisms/Strains		
Mouse: <i>Bapx1</i> ^{Cre}	Gift from Dr. Zimmer	<i>Nkx3-2</i> ^{tm1(cre)Wlez}
Mouse: <i>Sufu</i> ^{floxed}	Li et al., 2012	<i>Sufu</i> ^{tm1Hui}
Mouse: <i>Spop</i> ^{floxed}	WTSI KOMP	<i>Spop</i> ^{tm1c(KOMP)Wtsi}
Mouse: <i>Fat4</i> ^{-/-}	Saburi et al., 2008	<i>Fat4</i> ^{tm1.1Hmc}
Mouse: <i>Fat4</i> ^{floxed}	Saburi et al., 2008	<i>Fat4</i> ^{tm1Hmc}
Mouse: <i>Dchs1</i> ^{-/-}	Mao et al., 2011	<i>Dchs1</i> ^{tm1.2lv}
Mouse: <i>Vangl2</i> ^{LP}	Montcouquiol et al., 2003	<i>Vangl2</i> ^{LPT/LeJ}
Mouse: <i>Wnt5a</i> ^{-/-}	Cervantes et al., 2009	<i>Wnt5a</i> ^{tm1Amc}
Mouse: <i>Pdgfra</i> ^{H2B-eGFP}	Hamilton et al., 2003	<i>Pdgfra</i> ^{tm11(EGFP)Sor}
Oligonucleotides		
RNAscope Probe- Mm-Fat4	Advanced Cell Diagnostics	Cat# 447511
RNAscope Probe- Mm-Vangl1	Advanced Cell Diagnostics	Cat# 467481
RNAscope Probe- Mm-Vangl2	Advanced Cell Diagnostics	Cat# 316781
RNAscope Probe- Mm-Dchs1	Advanced Cell Diagnostics	Cat# 447501
RNAscope Probe- Mm-Ctgf	Advanced Cell Diagnostics	Cat# 314541
RNAscope Probe- Mm-Wnt5a	Advanced Cell Diagnostics	Cat# 316791
See Table S2 for primer sequences		
Recombinant DNA		
Plasmid: Fat4Pk1-fragment luciferase reporter	This paper	N/A
Plasmid: Fat4Pk2-fragment luciferase reporter	This paper	N/A
Plasmid: Vangl1Pk1-fragment luciferase reporter	This paper	N/A
Plasmid: Vangl1Pk2-fragment luciferase reporter	This paper	N/A
Plasmid: Vangl2Pk1-fragment luciferase reporter	This paper	N/A
Plasmid: Vangl2Pk2-fragment luciferase reporter	This paper	N/A
Plasmid: pRL-TK control	Promega	Cat# E2241
Plasmid: pCMV-Gli2-FLAG	Ding et al., 1999	N/A
Plasmid: pδ51LucII	Kamachi and Kondoh, 1993	N/A
Plasmid: pcDNA5-T/O-Ds1-mCherry	Loza et al., 2017	Addgene plasmid # 112855; RRID: Addgene_112855
Plasmid: pEv-Fat4-citrine	Loza et al., 2017	Addgene plasmid # 112854; RRID: Addgene_112854
Software and Algorithms		
ImageJ	NIH	N/A
GraphPad Prism	GraphPad	N/A
Kallisto	Bray et al., 2016	https://github.com/pachterlab/kallisto
DESeq2	Love et al., 2014	http://bioconductor.org/packages/release/bioc/html/DESeq2.html
PANTHER 14.0	Mi et al., 2019 Mi et al., 2013	http://www.pantherdb.org/
REVIGO	Supek et al., 2011	http://revigo.irb.hr/
Trimmomatic	Bolger et al., 2014	http://www.usadellab.org/cms/?page=trimmomatic
BWA-MEM	Li and Durbin, 2009	http://bio-bwa.sourceforge.net/
Bamtools	Barnett et al., 2011	https://github.com/pezmaster31/bamtools

(Continued on next page)

Continued

REAGENT or RESOURCE	SOURCE	IDENTIFIER
MACS2	Zhang et al., 2008	https://github.com/taoliu/MACS
BEDTools	Quinlan and Hall, 2010	N/A
Imaris	Oxford Instruments	N/A
Matlab	MathWorks	N/A
Drift compensation algorithm	This paper	https://github.com/MinZhuUOTSickKids/Intestinal-development-cell-tracking
FlowJo v10	BD	N/A

LEAD CONTACT AND MATERIALS AVAILABILITY

Further information and requests for resources and reagents should be directed to and will be fulfilled by the Lead Contact, Tae-Hee Kim (tae-hee.kim@sickkids.ca). All unique/stable reagents generated in this study are available from the Lead Contact without restriction.

EXPERIMENTAL MODEL AND SUBJECT DETAILS**Animals**

All animal husbandry was in accordance to the standards of the Canadian Council on Animal care, approved by institutional animal care committees by The Centre for Phenogenomics, Toronto. Housed mice were subjected to 12-hour dark-light cycles, fed standard rodent chow and had access to water at all times. Mice of either sex were used for all experiments, since to our knowledge there are no reported sex differences for villus morphogenesis. Therefore, mice of either sex were randomly assigned to each experimental group. *Sufu^{floxed}* and *Spop^{floxed}* mice have been previously described (Li et al., 2012) and accessed from the KOMP (trans-NIH knock-out mouse project) Repository (www.komp.org) respectively. *Fat4^{-/-}* (KO), *Fat4^{floxed}*, *Dchs1^{-/-}* (KO), *Vangl2^{Lp}*, *Wnt5a^{-/-}* (KO), *Pdgfra^{H2B:eGFP/+}* and *Bapx1^{Cre/+}* were previously described (Cervantes et al., 2009; Hamilton et al., 2003; Mao et al., 2011; Montcouquiol et al., 2003; Saburi et al., 2008; Verzi et al., 2009). *Bapx1^{Cre/+}* mice were graciously gifted from Dr. Warren Zimmer's group. For embryonic studies, observed plug date was considered embryonic day 0.5. All *Fat4-Dchs1*, *Pdgfra* reporter and PCP mutant lines were maintained as heterozygotes under mixed backgrounds for breeding, and subsequent homozygous embryos were generated by crossing 2 heterozygotes. To generate *Bapx1^{Cre/+};Fat4^{fl/-}* E15.5 embryos, *Bapx1^{Cre/+};Fat4^{fl/+}* mice were crossed to *Fat4^{+/-}* mice.

Cell Lines

C3H10T1/2 mouse embryonic fibroblast cells (ATCC #CCL-226) were cultured in the following conditions: Dulbecco's Modified Eagle's Medium (DMEM Invitrogen Cat# 11965-092) supplemented with 10% fetal bovine serum (Sigma-Aldrich Cat# F1051), penicillin and streptomycin, grown at 37°C with 5% CO₂. Information pertaining to the sex of this cell line is unavailable.

METHOD DETAILS**RNA-seq and ChIP-seq****Next-Generation Sequencing**

Next-generation sequencing experiments were performed as 126-bp paired-end reads on the Illumina HiSeq 2500 platform at the Centre for Applied Genomics (TCAG) – The Hospital for Sick Children Toronto.

RNA Sequencing

Bapx1^{Cre/+};Sufu^{fl/fl};Spop^{fl/fl} intestines and littermate controls at E17.5 were harvested and isolated for mesenchymal tissue by 10mM EDTA shaking at 4°C (Coquenlorge et al., 2019). RNA extraction was performed using the RNeasy kit (Qiagen). Poly-A mRNA libraries were prepared with 1–2µg RNA with RIN>8.5 (determined on Agilent Bioanalyzer). Kallisto 0.42.2 and DESeq2 package were used to align reads to mouse mm9 reference transcriptome, summarize gene expression levels and perform differential gene expression analysis, respectively (Bray et al., 2016; Love et al., 2014; Sonesson et al., 2015). For GO term analysis, a PANTHER 14.0 overrepresentation test (Fisher's exact) with all GO biological processes of upregulated genes from RNA-seq (cut off: 2-fold, p<0.05) were used (Mi et al., 2017, 2013, 2019). The top 300 upregulated GO terms from this test were inputted in the REVIGO platform to remove redundant GO terms, and outputted as a scatterplot to visualize similarity and representation of biological functions (Supek et al., 2011) (refer to Table S1 for list of GO terms).

ChIP Sequencing

Whole intestines were harvested from *Bapx1^{Cre/+};Sufu^{fl/fl};Spop^{fl/fl}* mutants at E17.5 in duplicate (Coquenlorge et al., 2019). Samples were prepared as described in Schmidt et al. (2009). GLI2 (Cheung et al., 2009), H3K27Ac (Millipore, 05-1334) and H3K36me3 (Abcam, ab9050) antibodies were used. The NEBNext Ultra DNA library preparation kit and NEBNext Multiplex Oligos for Illumina (New England Biolabs) were used for library preparation. Trimmomatic 0.35 (Bolger et al., 2014) and BWA-MEM (Li and Durbin,

2009) with default parameters were used for adaptor sequence trimming and alignment to the mouse mm9 reference genome respectively. Bamtools (Barnett et al., 2011) was used to select uniquely mapped reads with mapping quality cut-off > 5. BEDTools (Quinlan and Hall, 2010) and MACS2 (Zhang et al., 2008) were used to remove ENCODE-recommended blacklist regions and peak calling respectively. Input DNA was used as control, with parameters -g mm -f BAMPE -keep-dup auto -q 0.05 for GLI2, and additionally -broad for histone marks.

ChIP Peak Validation

GLI2 peak sequences for *Fat4*, *Vangl2* and *Vangl1* were cloned into the pδ51LucII plasmid, upstream of the luciferase reporter (Kamachi and Kondoh, 1993). C3H10T1/2 mouse embryonic fibroblast cells (ATCC-CCL-266) were co-transfected with reporter, and pRL-TK renilla control (Promega), with or without the *Gli2* expression plasmid (Ding et al., 1999) (n=3). Transfected cells were harvested 36 h later and measured for bioluminescence using the Dual Luciferase Reporter Assay System (Promega E1910) and Molecular Devices Spectramax L luminometer.

Electron Microscopy, Histology and Immunostaining

Scanning Electron Microscopy

After dissection, E15.5 intestinal samples were placed in 2% glutaraldehyde in 0.1M sodium cacodylate buffer pH 7.3 for overnight fixation at 4°C. Ethanol-dehydrated samples were critical-point dried and attached to aluminum stubs for gold-sputter coating. Images were acquired on an FEI XL30ESEM system at the Nanoscale Biomedical Imaging Facility at the Hospital for Sick Children, Toronto.

Histology and Immunofluorescence

After dissection, intestinal samples were fixed in 4% paraformaldehyde, dehydrated in ethanol and embedded in paraffin. Tissues were sectioned at 5µm thickness and deparaffinized and rehydrated using standard techniques (xylene and descending ethanol gradients). For H&E, tissues were stained with Harris' Hematoxylin and alcoholic Eosin Y. For IF, sections were subjected to antigen retrieval (99°C for 15 min in 10mM sodium citrate, pH 6 solution) followed by 1 h blocking (10% goat serum, 0.1% triton-X in PBS) at room temperature. Primary antibodies were applied at 4°C and incubated overnight. The following antibodies were used: rabbit anti-alpha smooth muscle actin 1:1,000 (Abcam, ab124964), mouse anti-alpha smooth muscle actin 1:500 (Abcam, ab7817), rabbit anti-SM22 1:500 (Abcam, ab14106), rabbit anti-PDGF receptor alpha C-20 1:200 (Santa Cruz Biotechnology, sc-338), rabbit anti-VANGL2 1:50 gifted from Dr. Philippe Gros (Leung et al., 2016), mouse anti-PCNA 1:200 (Santa Cruz Biotechnology, sc-56) and mouse anti-EZRIN 1:1000 (Sigma-Aldrich E8897). For IF, secondary antibodies were applied for 1 h at room temperature with Alexa Fluor 488- and 568-conjugated (1:500, Thermo Fisher) and mounted with Fluoroshield Mounting Medium with DAPI (Abcam, ab104139). For F-actin staining, tissues were cryo-sectioned and hydrated with PBS, followed by 1 h of blocking and 1 h of staining with Alexa Fluor 568-conjugated Phalloidin 1:1000 (Thermo Fisher A12380) at room temperature. The images were taken on Nikon E1000 epifluorescence and Nikon A1R confocal microscopes.

Western Blot

Snap frozen E15.5 intestinal tissue (1 whole intestine per n, n=3) was lysed in ice cold RIPA buffer, supplemented with protease and phosphatase inhibitor cocktails (Roche 4693132001 and Roche 4906845001), using a Mini-BeadBeater-16 (Biospec Products). Homogenized tissue was subjected to sonication using a Bioruptor (Diagenode) for 5 cycles (30 seconds on/ 30 seconds off). Lysates were centrifuged and supernatant was kept at -80°C until the time of western blot. Protein was quantified using the Pierce BCA Protein Assay Kit (Thermo Fisher Scientific 23225) and 11µg were boiled and loaded with laemmli buffer in each lane of a 4-15% Tris-Glycine precast gel (Biorad 4561086). Migrated proteins were transferred to PVDF membranes, overnight at 4°C, using a wet electroblotting system (Mini Trans-Blot Cell, Bio-Rad). Membranes were blocked with 5% bovine serum albumin (BSA) in Tris-buffered saline-0.1% tween (TBST) for 1 h at room temperature, followed by overnight incubation with primary antibodies: rabbit anti-YAP 1:1000 (Cell Signaling Technology 14074), rabbit anti-PhosphoYAP 1:1000 (Cell Signaling Technology 4911), rabbit anti-GAPDH 1:10000 (Abcam 181602) and rabbit anti-H3K27me3 1:1000 (Millipore 07-449), diluted in blocking solution. Blots were washed, then incubated with HRP-conjugated secondary antibodies at 1:10000 (Thermo Fisher Scientific 31460) for 1 h at room temperature. Chemiluminescence was produced using the SuperSignal West Femto Substrate kit (Thermo Fisher Scientific 34095) and imaged using a Licor Odyssey Fc system. YAP and Phospho-YAP were quantified using ImageJ by normalizing to GAPDH levels for each lane.

RNA Quantification and Visualization

Quantitative PCR

Whole E15.5 intestinal tissue was homogenized using a Mini-BeadBeater-16 (Biospec Products) in TRIzol reagent (Thermo Fisher Scientific 15596026). After addition of chloroform and centrifugation, RNA was extracted from the aqueous phase, by precipitating with isopropanol, and washing with 70% ethanol, according to manufacturer's protocol. Pelleted RNA was solubilized in RNase free water. All cDNA was synthesized using SuperScript III First-Strand synthesis kit (Thermo Fisher Scientific, 11752050). qPCR was performed using the Power SYBR Green PCR Master Mix with 20ng of cDNA per reaction (10-µL reaction volume) and run on ViiA 7 Real-Time PCR System, Applied Biosystems. Fold changes were calculated using the $\Delta\Delta C_T$ method. Refer to Table S2 for all primer sequences.

SmFISH

Paraffin embedded tissues were sectioned at 5 μ m and used for single-molecule fluorescence in situ hybridization (smFISH) following the RNAscope Multiplex Fluorescence Detection Kit v2 (323110) protocol by Advanced Cell Diagnostics. Probes were also purchased and designed by Advanced Cell Diagnostics. The following RNA probes were used: *Fat4* (447511), *Ctgf* (314541), *Vangl1* (467841), *Vangl2* (316781), *Dchs1* (447501) and *Wnt5a* (316791). Images were acquired on Nikon Epifluorescence TE-2000, Nikon E1000, Nikon A1R confocal and Leica SP8 confocal microscopes.

Cell Isolation and Sorting

Epithelial and Mesenchymal Cell Isolation

Wildtype E15.5 intestines were harvested and pooled (2 embryos per sample) for a total of n=4 (8 embryos) from 2 different litters. The intestines were micro-dissected and cut open to expose epithelium in a 10mM EDTA solution. Samples were agitated for 30 min at 4 $^{\circ}$ C to separate epithelium from mesenchyme and muscle layer. This supernatant (epithelium) and mesenchymal fractions were washed in PBS:2%FBS, and resuspended in RNeasy lysis solution at -20 $^{\circ}$ C until the time of RNA isolation. RNA was isolated using the RNeasy mini kit (Qiagen, 74104).

Cell Sorting

Pdgfra^{H2B:eGFP/+} (control) and *Pdgfra*^{H2B:eGFP/+};*Fat4* KO E15.5 intestines were harvested in HBSS and micro-dissected in ice cold PBS:2%FBS (pooled between 1-7 intestines per sample). Tissue was digested with TrypLE express (Thermo Fisher Scientific 12604013) diluted 2:1 in PBS at 37 $^{\circ}$ C for 6 min. Once tissue was soft, it was manually digested with P200 pipette at room temperature until a single cell suspension was observed. Cells were then washed in PBS:2%FBS, resuspended in Sytox Blue (1:5000), and then passed through a 35- μ m nylon mesh before being put through either Beckman Coulter MoFlo Astrios, VBYR or Sony SH800 BRV instruments. GFP+ populations were collected from the live cells (refer to [Figures S5A](#) and [S5B](#) for sorting scheme). To collect EPCAM-/GFP- cells, after digestion, samples were resuspended in primary antibody EpCAM-APC (Abcam ab95641) at 1:100. Cells were stained for 20 min on ice, washed in PBS:2%FBS, and resuspended in Sytox Blue (1:5000). GFP-/EPCAM- populations were collected from the live cells ([Figure S5C](#)). Results were analyzed with FlowJo v10 software.

Live Imaging

Live Lightsheet Imaging

Pdgfra^{H2B:eGFP/+} (control) and *Pdgfra*^{H2B:eGFP/+};*Fat4* KO E13.5 intestines were harvested in ice cold HBSS and micro-dissected in ultrapure PBS (n=3 for control, n=4 for mutants). Intestines (gut completely intact, with stomach and colon) were placed in 6-well transwell, supplemented with growth media (DMEM with 10% FBS and Pen/Strep) in the upper and lower chambers and incubated at 37 $^{\circ}$ C with 5% CO₂. After 24 h in culture, each intestine was embedded in a solution of DMEM (no phenol red) containing 12.5% FBS, 1% low melt ultrapure agarose (Invitrogen) and 2% of fluorescence bead solution (SigmaAldrich, 1:500, diameter 500nm). The agarose solution-immersed intestine was embedded into a glass capillary tube and was submerged into an imaging chamber containing DMEM (no phenol red) after the agarose solidified. The agarose-embedded intestine was plunged out of the capillary tube directly into the media inside the imaging chamber. The temperature of the imaging chamber was maintained at 37 $^{\circ}$ C with 5% CO₂. Images were acquired using a 20 \times /1 objective with dual-side illumination for 3 h with 150-ms intervals on a Zeiss Lightsheet Z1 microscope.

Drift-Compensated Cell Tracking

The light sheet time-lapse image was first rendered in Imaris (Bitplane). Using the fluorescent beads that were embedded in the agarose along with the tissue sample, it was possible to subtract any drift that occurred during the imaging time frame (3 h). The positions of cell nuclei and fluorescent beads were tracked over time using an autoregressive motion algorithm, from frames with the same peristaltic wave phase. The tracking/positional data were then imported into R2017b Matlab (MathWorks) for drift compensation and visualization (cell trajectories and net cell displacement) using a customized algorithm available at <https://github.com/MinZhuJOTSickKids/Intestinal-development-cell-tracking>.

In Vitro Assays

Spheroid Formation Assay

GFP+ cells from *Pdgfra*^{H2B:eGFP/+} (control) and *Pdgfra*^{H2B:eGFP/+};*Fat4* KO samples, and GFP-/EPCAM- cells from controls were resuspended at a concentration of 10,000 cells/ μ L growth media (DMEM with 10% FBS and Pen/Strep). 96-well plates were coated with 50 μ L of Matrigel (Corning, CACB456231) per well, and left to solidify for approximately 1 min. In each well, 5 μ L of cell suspension (control or mutant) were added directly into the center of the Matrigel, and left to solidify in the incubator at 37 $^{\circ}$ C with 5% CO₂ for 30 min. Wells were topped up with 100 μ L of growth media above the Matrigel, kept in the incubator at 37 $^{\circ}$ C with 5% CO₂, and maintained by media changes every 2-3 days (n=3 biological samples, 7 wells for control, 6 wells for mutant). For staining, spheroids were fixed with 4% paraformaldehyde for 10 min at room temperature, followed by blocking (10% goat serum, 0.1% triton-X in PBS) and overnight incubation at 4 $^{\circ}$ C with mouse anti-PCNA 1:100 (Santa Cruz Biotechnology, sc-56). Alexa Fluor 488-conjugated secondary antibody 1:500 (Thermo Fisher) and DAPI (1:1000) were applied for 1 h at room temperature, followed by storage in 50% glycerol:PBS solution for imaging and acquisition on Nikon Epifluorescence TE-2000 microscope. Spheroids were scored based on their spherical morphologies and were quantified at day 5 (reported as absolute number and size of spheroids per well).

Transwell Migration Assay

Sorted GFP+ cells from *Pdgfra*^{H2B:eGFP/+} (control) and *Pdgfra*^{H2B:eGFP/+}; *Fat4* KO samples were resuspended in serum free DMEM with 0.1% BSA and Pen/Strep at a concentration of 500 cells/ μ L. 24-well transwells with 8 μ m pore sizes were prepared by adding either recombinant WNT5A (R&D Systems, 645-WN-010) at 0.1 μ g/ml, or BSA vehicle control to DMEM with 0.1% BSA to the lower chamber of the transwell. 100 μ L of the cell suspension was added to the upper chamber of each transwell. Cells were incubated at 37°C with 5% CO₂ for 36 h. For cyclopamine treatment, sorted GFP+ cells from control samples were resuspended in 5 μ M of cyclopamine or vehicle control in serum free DMEM with 0.1% BSA at a concentration of 500 cells/ μ L. 100 μ L of the treated cell suspension was added in the upper chamber, with 0.1 μ g/ml of WNT5A in the lower chamber, and allowed to migrate for 36 h at 37°C with 5% CO₂. Cells that migrated through transwell were fixed with 4% paraformaldehyde, stained with DAPI and imaged on a Nikon E1000 microscope for quantification (n=3 biological samples, at least 2 technical replicates each).

Primary Cell Culture and Transfection

Sorted GFP+ cells from *Pdgfra*^{H2B:eGFP/+} intestines were cultured in DMEM supplemented with 10% FBS, non-essential amino acids, glutamine and pen/strep and allowed to adhere overnight. Cells were then transfected with 1 μ g of empty vector (CMV) or *FAT4* and *DCHS1* overexpression vectors using Lipofectamine 3000. pEv-Fat4-citrine and pcDNA5-T/O-Ds1-mCherry were a gift from David Sprinzak (Addgene plasmid # 112854 ; <http://n2t.net/addgene:112854> ; RRID:Addgene_112854, Addgene plasmid # 112855 ; <http://n2t.net/addgene:112855> ; RRID:Addgene_112855 respectively) (Loza et al., 2017). 24 h post-transfection, 50,000 cells were resuspended in 100 μ L of serum free DMEM with 0.1% BSA, doxycycline (100ng/ml) and either vehicle control (100% ethanol) or cyclopamine (5 μ M) and subjected to transwell migration assay with WNT5A (n=3 biological replicates).

QUANTIFICATION AND STATISTICAL ANALYSIS

All quantifications are displayed as mean \pm standard error of the mean, where the statistical parameters are reported in the [STAR Methods](#) or corresponding figure legends. Two-tailed *P*-values were calculated using parametric unpaired Student's *t* test. *P*<0.05 was considered statistically significant.

DATA AND CODE AVAILABILITY

Accession numbers for the ChIP and RNA-seq (Coquenlorge et al., 2019) referenced in this paper:

GEO: GSE103683 (RNA-seq). GEO: GSE103690 (ChIP-seq).

The drift compensation algorithm generated during this study is available at: <https://github.com/MinZhuUOTSickKids/Intestinal-development-cell-tracking>.